iScience

CellPress
OPEN ACCESS

Article

COP I and II dependent trafficking controls ER-associated degradation in mammalian cells

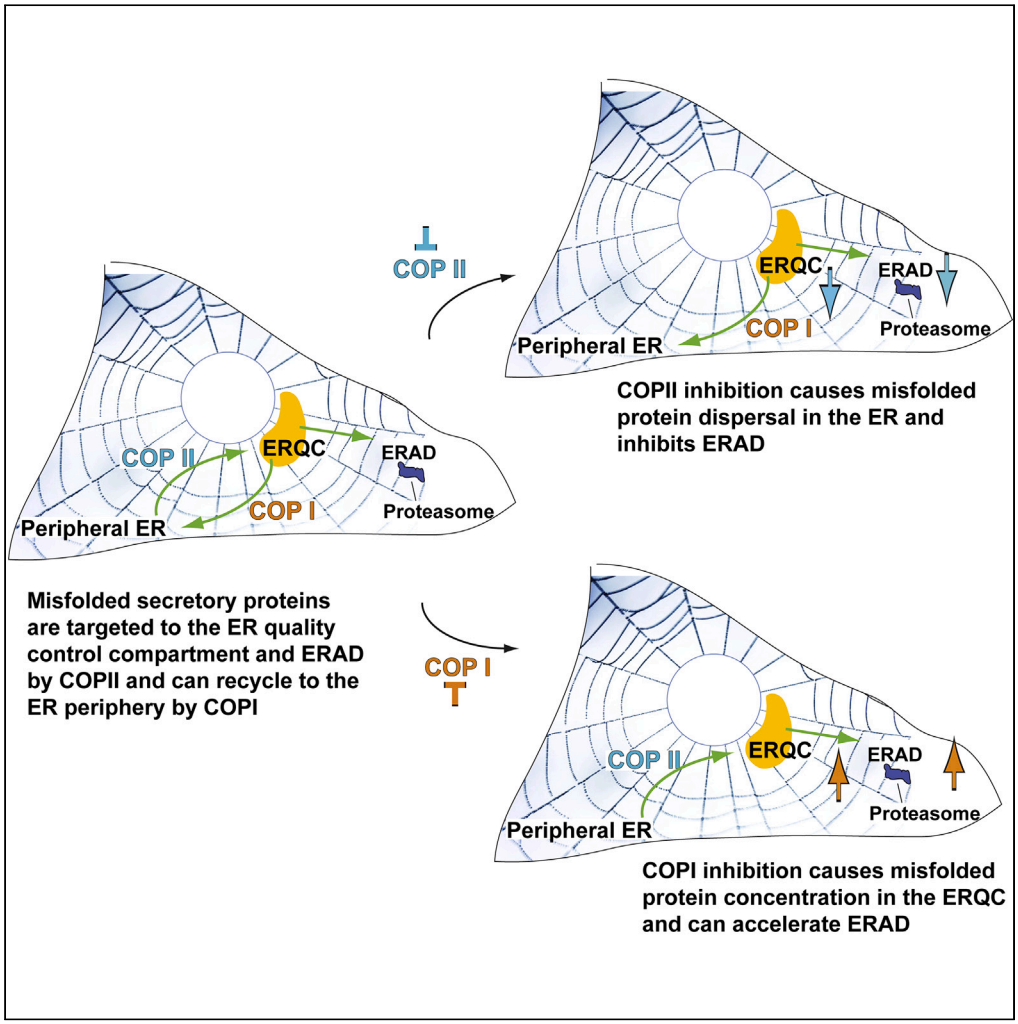

Navit Ogen-Shtern, Chieh Chang, Haddas Saad, Niv Mazkereth, Chaitanya Patel, Marina Shenkman, Gerardo Z. Lederkremer

gerardol@tauex.tau.ac.il

Highlights

The ER quality control compartment (ERQC) targets misfolded proteins to degradation

Trafficking to the ERQC and recycling to the ER require vesicular trafficking

COPII is involved in trafficking to the ERQC for ER-associated degradation (ERAD)

COPI is required for protein recycling from the ERQC to the peripheral ER

Ogen-Shtern et al., iScience *26*, 106232
March 17, 2023
https://doi.org/10.1016/j.isci.2023.106232

iScience

CellPress
OPEN ACCESS

Article

COP I and II dependent trafficking controls ER-associated degradation in mammalian cells

Navit Ogen-Shtern,[1,2,3,4] Chieh Chang,[1,2,4] Haddas Saad,[1,2,4] Niv Mazkereth,[1,2] Chaitanya Patel,[1,2] Marina Shenkman,[1,2] and Gerardo Z. Lederkremer[1,2,5,*]

SUMMARY

Misfolded proteins and components of the endoplasmic reticulum (ER) quality control and ER associated degradation (ERAD) machineries concentrate in mammalian cells in the pericentriolar ER-derived quality control compartment (ERQC), suggesting it as a staging ground for ERAD. By tracking the chaperone calreticulin and an ERAD substrate, we have now determined that the trafficking to the ERQC is reversible and recycling back to the ER is slower than the movement in the ER periphery. The dynamics suggest vesicular trafficking rather than diffusion. Indeed, using dominant negative mutants of ARF1 and Sar1 or the drugs Brefeldin A and H89, we observed that COPI inhibition causes accumulation in the ERQC and increases ERAD, whereas COPII inhibition has the opposite effect. Our results suggest that targeting of misfolded proteins to ERAD involves COPII-dependent transport to the ERQC and that they can be retrieved to the peripheral ER in a COPI-dependent manner.

INTRODUCTION

During secretory protein biogenesis, after translocation into the ER, the quality control machinery facilitates protein folding and promotes segregation of misfolded proteins destined for ERAD. We had previously determined that misfolded proteins destined to ERAD accumulate in a specialized pericentriolar compartment, the ER-derived quality control compartment (ERQC), a staging ground for retrotranslocation and targeting to ERAD.[1–5] The ERAD-associated luminal lectin OS-9 always appears localized mainly at the ERQC, whereas other quality control and ERAD components are recruited on misfolded protein accumulation (ER stress). This compartmentalization depends on the PERK pathway of the unfolded protein response (UPR) and on the upregulation of Herp.[4] PERK is activated by the initial accumulation of misfolded proteins and consequently upregulates Herp, resulting in a dynamic protein recruitment to the ERQC. Herp recruits the membrane-bound ubiquitin ligase HRD1 and additional quality control and ERAD machinery components, such as the luminal calreticulin (CRT), and the membrane proteins calnexin (CNX), Derlin-1, EDEM1, ERManI and cytosolic components, including the ubiquitin ligase SCFFbs2 and the AAA ATPase p97.[2,6,7] However, other machinery proteins such as BiP, PDI, UGGT and ERp57, do not accumulate in the ERQC.[2–5,8,9] Here we show that compartmentalization of ERAD substrates in the ERQC, and subsequent targeting to ERAD, depend on a mechanism that is consistent with vesicular trafficking, involving coat protein complex II (COPII), and that recycling from the ERQC requires COPI. COPI and COPII coats had first been identified as complexes that take part in vesicular trafficking between the ER and the Golgi.[10–12] Yet, COPII was recently found to participate in other processes taking place from the ER as well, including the formation of ER whorls in mammalian cells[13] and an autophagy process targeting the ER (ER-phagy) in yeast.[14,15]

RESULTS

Dynamics of concentration of ER quality control and ERAD components at the ERQC on proteasomal inhibition

We had previously shown that on proteasomal inhibition with diverse inhibitors, or under other conditions in which ERAD substrates accumulate (ER stress), several ER quality control and ERAD factors concentrate at the ERQC. This can be seen, for example, by comparing the localization of an established ERAD substrate, the uncleaved precursor of asialoglycoprotein receptor H2a, linked to monomeric red fluorescent protein (H2a-RFP), which serves as a marker of the ERQC,[3,4] with that of the soluble luminal chaperone

[1]The Shmunis School of Biomedicine and Cancer Research, Cell Biology Division, George Wise Faculty of Life Sciences, Tel Aviv University, Tel Aviv 69978, Israel

[2]Sagol School of Neuroscience, Tel Aviv University, Tel Aviv 69978, Israel

[3]Present address: The Skin Research Institute, The Dead-Sea and Arava Science Center, Masada 86910, Israel

[4]These authors contributed equally

[5]Lead contact

*Correspondence: gerardol@tauex.tau.ac.il

https://doi.org/10.1016/j.isci.2023.106232

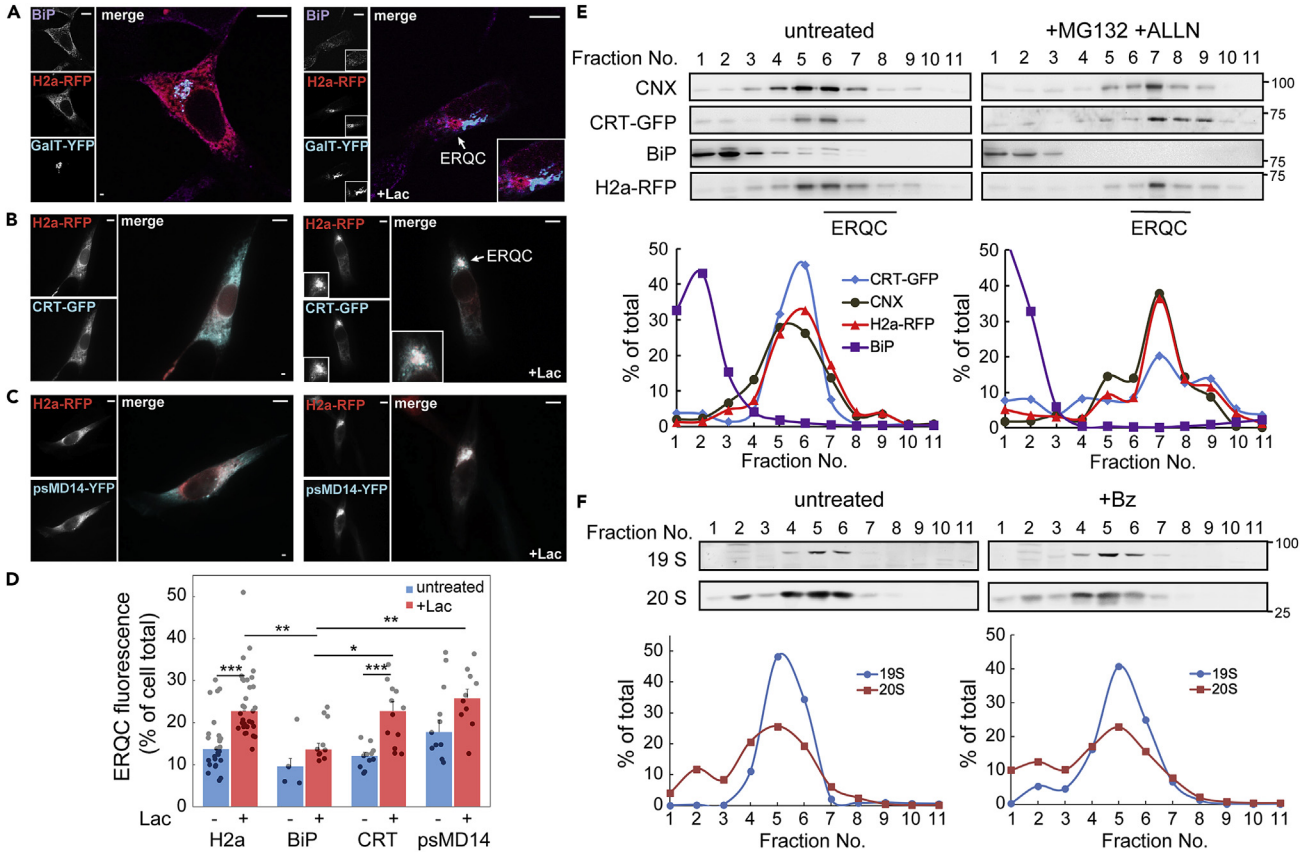

Figure 1. ERAD substrate H2a-RFP, CRT-GFP and proteasomes accumulate at the ERQC on proteasomal inhibition

(A–C) Fluorescence microscopy of NIH3T3 cells treated without or with the proteasomal inhibitor Lactacystin (Lac, 20 μM, 3h), transiently expressing H2a-RFP and the Golgi marker GalT-YFP (A), CRT-GFP (B), or psMD14-YFP (C). CRT-GFP (B) and the proteasomal subunit psMD14-YFP (C) concentrate and colocalize with H2a-RFP at the juxtanuclear ERQC, especially in Lac-treated cells. In contrast, there is no colocalization of H2a-RFP with GalT-YFP and no concentration of BiP in Lac-treated cells (A). Bars= 10μm.

(D) The percentage of fluorescence in the ERQC compared to the entire cell was measured in the cells in (A-C) (see STAR Methods and Figure S2). The graph shows mean ±SEM of cells from three independent experiments (10–30 cells per population). p value +Lac versus untr.: H2a-RFP= 4.8 x 10^{-6}, CRT-GFP= 0.00027; versus BiP + Lac: H2a-RFP= 0.0015, CRT-GFP= 0.029, psMD14-YFP= 0.0013.

(E) Immunoblots of fractions of iodixanol density gradients from NIH3T3cells transiently expressing CRT-GFP and H2a-RFP show comigration of CRT-GFP, H2a-RFP and endogenous CNX in mid-density fractions (5–7), shifting to denser fractions (6–8) (ERQC) on MG-132 + ALLN (50 μM, 3h) treatment, compared to untreated cells. BiP appears in lighter fractions and does not shift on proteasomal inhibition. MW markers in kDa are indicated on the right. The graphs show quantification of the percentage of the signal in each fraction relative to the sum of all fractions. The experiment is representative of 3 independent repeat experiments.

(F) In a similar experiment, most of the endogenous proteasome subunits 19S and 20S appear in similar mid-density fractions upon iodixanol fractionation. In this case proteasomal inhibition was done for 3h with Bz (1 μM). Representative of 3 independent repeat experiments.

See also Figures S1 and S2.

BiP in NIH3T3 cells. Whereas H2a-RFP was recruited to the ERQC under proteasomal inhibition with lactacystin (Lac), BiP was not (Figure 1A), as we had previously seen.[16] H2a-RFP accumulates in the centrosomal region of the cell but with no colocalization with a Golgi marker, GalT-YFP[2,3] (Figure 1A). In contrast to BiP or BiP linked to GFP (BiP-GFP) (Figure S1), another soluble luminal chaperone, CRT linked to GFP (CRT-GFP) was recruited to the ERQC under proteasomal inhibition (Figure 1B). A proteasomal subunit linked to YFP, PSMD14-YFP, was also partially recruited to the ERQC region on proteasomal inhibition (Figure 1C), similarly to what we had seen with other cytosolic ERAD factors, p97 and SCF^{Fbs2}.[3,7] PSMD14-YFP even showed a higher presence in the ERQC region than H2a-RFP and CRT-GFP in untreated cells (Figures 1D and S2). Using another approach to analyze the compartmentalization, iodixanol gradients optimized to separate the different ER-like densities,[4,6] we observed H2a-RFP peaking in middle fractions (5-6), with a small shift to heavier fractions, peaking in fraction 7, on proteasomal inhibition, in this case with a combination of MG132 and ALLN (Figure 1E). We had previously characterized this shift as occurring on

protein concentration in the ERQC.[4,6] CRT-GFP had a similar behavior and also endogenous CNX. In contrast, endogenous BiP appeared in the light fractions and its migration did not change on proteasomal inhibition. Consistent with the fluorescence of PSMD14-YFP, most of the endogenous proteasomes, likely membrane-bound, detected with antibodies against the 19S and 20S proteasomal subunits, also appeared in the middle fractions, with a lesser shift on proteasomal inhibition, in this case with the proteasome inhibitor bortezomib (Bz) (Figure 1F). Therefore, using different approaches and various proteasome inhibitors we can observe accumulation in the ERQC of an ERAD substrate, proteasomes and some chaperones at the ERQC.

To analyze the dynamics of protein concentration at the ERQC, we performed a live cell time-lapse experiment with cells expressing H2a-RFP and CRT-GFP. In this case, we used CHO cells, which are less mobile, to facilitate measurements for several hours. A stable cell line expressing CRT-GFP was established, which was transfected with H2a-RFP and treated with Lac for 3h, during which we conducted live cell imaging (Figure 2A). Both H2a-RFP and CRT-GFP concentrated in the ERQC during this period, although a larger portion of CRT-GFP remained in the peripheral ER compared to H2a-RFP (Figures 2A and 2B). H2a-RFP concentrated in the ERQC at a rate of 13% of the total cellular protein per minute, whereas the rate for CRT-GFP was 4.1% per minute, a 3.25-fold slower rate (Figure 2B).

The interaction of CRT with its glycoprotein substrates is dependent on a functional lectin domain. We established a stable cell line expressing CRT(Y108F)-GFP, which carries a point mutation in its lectin domain.[17] A time lapse experiment similar to the one described above using WT CRT-GFP was performed with this mutant (mutCRT-GFP). Although H2a-RFP concentrated in the ERQC of these cells as before, although at a slower rate (6.6% per min), mutCRT-GFP did not concentrate to any significant extent within the 3h time frame (1.1% per min) (Figures 2C and 2D). Although the rate of protein concentration varied to some extent in repeat experiments, mutCRT-GFP did not accumulate in the ERQC (Figure S3).

We compared the colocalization by calculating the Pearson's coefficient. For WT CRT-GFP the colocalization with H2a-RFP increased with time, whether only the ERQC region or the entire cell were measured (light or dark blue trendlines respectively in Figure 2E). The colocalization measured for the entire cell area increased at a higher rate and to a higher extent than that measured for the ERQC, suggesting that colocalization of CRT-GFP and H2a-RFP already occurs in peripheral ER sites, before transport to the ERQC. In contrast, there was no colocalization and no increase with time for mutCRT-GFP (Figure 2E, orange and red trendlines) suggesting that the binding to substrates through its lectin domain is necessary for the accumulation of CRT in the ERQC. These results were not unique to the CHO cell lines, they were similar in NIH3T3 cells, where after 3h of Lac treatment mutCRT-GFP concentrated in the ERQC to a much lower extent than WT CRT-GFP (Figures 2F and 2G).

Recycling from the ERQC to the peripheral ER

To study the reversibility of the process of protein concentration in the ERQC, we treated cells expressing H2a-RFP and CRT-GFP with the reversible proteasome inhibitor MG-132 (as opposed to the covalent inhibitor Lac) for 3h, after which the inhibitor was removed by changing the medium (washout), and the cells were followed for up to another 2.5h. Both H2a-RFP and CRT-GFP accumulated in the ERQC after treatment, and the ERQC accumulation decreased significantly after washout (Figures 3A and 3B). For H2a-RFP, this decrease could be because of recycling to the peripheral ER or alternatively to its proteasomal degradation. However, in the case of CRT-GFP, as it is neither an ERAD substrate nor a short-lived protein, the reduction in its concentration at the ERQC must be ascribed to its recycling back to the peripheral ER.

To better understand the dynamics of recycling from the ERQC to the peripheral ER we performed a fluorescence loss in photobleaching experiment (FLIP) in live NIH3T3 cells expressing H2a-RFP and CRT-GFP under continuous proteasomal inhibition. Cells were treated with Lac for 3h for protein accumulation in the ERQC, after which both fluorescent proteins were repetitively bleached in a peripheral region of the ER. H2a-RFP fluorescence intensity in the ERQC declined throughout the time-lapse (Figure 3C and Video S1), though more slowly than in the ER periphery (Figure 3D). This indicates that H2a-RFP cycles back to the ER periphery, but the nature of the trafficking from the ERQC to the peripheral ER is slower than within the ER, suggesting that it is a vectorial movement, likely vesicular trafficking rather than diffusion. In addition, transient increases in fluorescence intensity in the ER periphery suggest uneven trafficking events, such as that occurring at around 200 s, with a concomitant decrease in the ERQC region (Figure 3D).

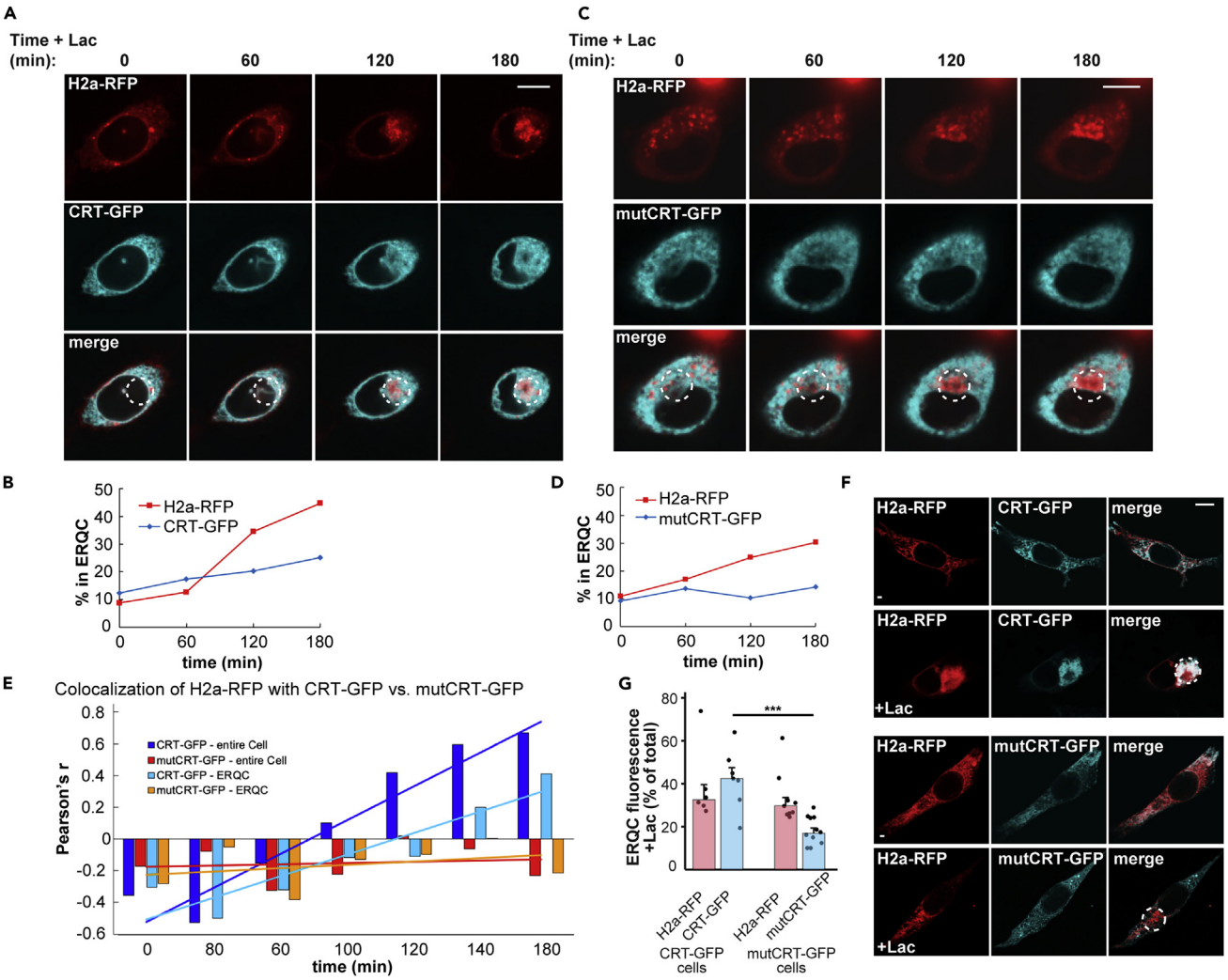

Figure 2. Movement of H2a-RFP and CRT-GFP to the ERQC. CRT-GFP dependence on its lectin activity

(A) CHO cells stably expressing CRT-GFP were transiently transfected with H2a-RFP and treated with Lac (10 μM). Live cell imaging shows the dynamic concentration of both proteins in the juxtanuclear ERQC. Bar= 10μm.

(B) The percentage of H2a-RFP and CRT-GFP concentrated in the ERQC (dashed circles in (A)) was calculated at the different time points.

(C and D) CHO cells stably expressing mutCRT-GFP, lacking a functional lectin domain, were transfected with H2a-RFP and treated with 10 μM Lac. Live cell imaging shows absence of mutCRT-GFP accumulation at the ERQC. Bar= 10μm.

(E) Pearson's coefficients of colocalization of CRT-GFP or mutCRT-GFP with H2a-RFP in the entire cell or in the area of the ERQC were measured at different time points in the experiments in (A) and (B). mutCRT-GFP showed no colocalization with H2a-RFP. The results are representative of 3 independent experiments.

(F) In Lac-treated NIH3T3 cells (20 μM, 3h), CRT-GFP and H2a-RFP accumulate in the ERQC, whereas untreated cells show an ER pattern. No colocalization appears in the ERQC (dashed circles) of NIH3T3 cells expressing mutCRT-GFP and H2a-RFP after incubation with Lac, compared to untreated cells. Bar= 10μm.

(G) The percentage of GFP or RFP fluorescence in the ERQC compared to the entire cell was measured in Lac-treated cells expressing CRT-GFP plus H2a-RFP or mutCRT-GFP plus H2a-RFP. The graph shows mean ±SEM of cells from two independent experiments (~20 cells per population). p value CRT-GFP versus mutCRT-GFP = 0.00014.

See also Figure S3.

The fluorescence intensity of CRT-GFP in the ERQC also declined more slowly than in the ER periphery (Figure 3E). Both CRT-GFP and H2a-RFP cycle back from the ERQC to the ER periphery in a non-diffusive manner. To compare the trafficking dynamics of H2a-RFP and CRT-GFP we calculated the ratio between the curve slopes (fluorescence loss rate) for each protein in the ER periphery and in the ERQC (Figures 3D and 3E). This ratio was more than 2-fold higher for H2a-RFP than for CRT-GFP when averaging

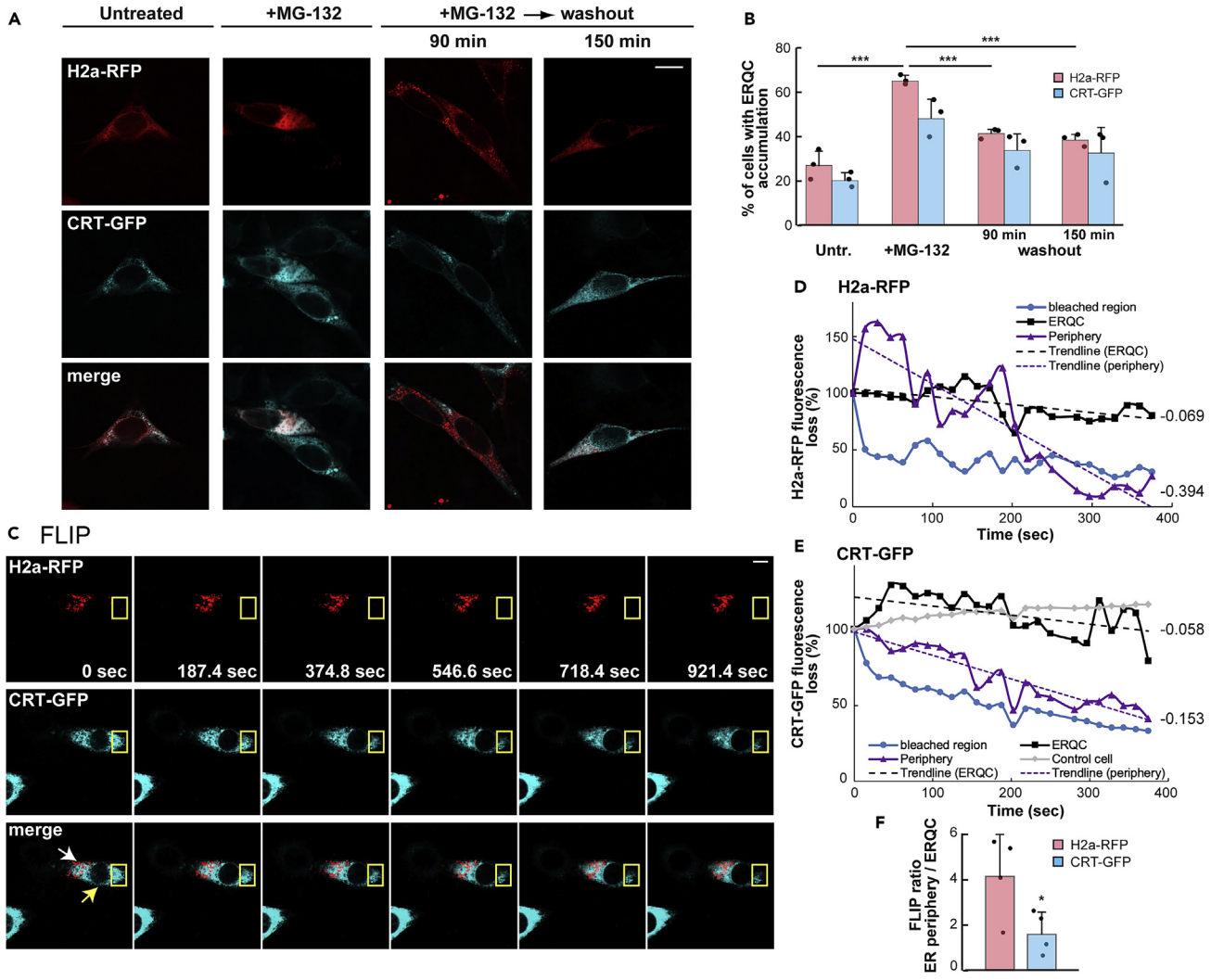

Figure 3. Recycling from the ERQC to the ER is slower than movement within the ER periphery

(A) NIH3T3 cells transiently expressing CRT-GFP and H2a-RFP treated with MG-132 (50 μM, 3h), followed by drug washout. The accumulation in the ERQC after treatment reverts to an ER pattern after washout. Bar= 10μm.

(B) Percent of cells with ERQC accumulation of H2a-RFP or CRT-GFP at the different times (see STAR Methods), average of 3 independent experiments ±SD. p values for H2a-RFP, +MG-132 versus untreated = 0.0007, 90 min washout versus +MG-132 =0.0002, 150 min washout versus +MG-132 =0.0002.

(C) Fluorescence loss in photobleaching (FLIP). Lac-treated NIH3T3cells (20 μM, 3h) were repetitively bleached in an ER periphery region (yellow rectangles) and scanned after each set of bleaching. Fluorescence intensity was measured at the ERQC (white arrow), the ER periphery (yellow arrow) and the bleached region. Bar= 10 μm. Representative of 4 experiments. See Video S1.

(D and E) Loss of the fluorescence intensity during FLIP compared to the start point for H2a-RFP (D) and for CRT-GFP (E), in the ERQC, ER periphery, bleached region and in a control cell, during the first 400 s. Recycling from the ERQC to the periphery is much slower than diffusion in the periphery. Fluorescence in the bleached region was lost quickly, whereas there was no non-specific bleaching of a nearby but non-irradiated control cell.

(F) Ratio between the FLIP curve slopes (calculated from linear trendlines) for each protein in the ER periphery compared to the ERQC, average of 4 independent experiments ±SD. p value = 0.049. The relative recycling rate from the ERQC is much slower for H2a-RFP than for CRT-GFP.

cells from repeat experiments (Figure 3F), indicating that the movement out of the ERQC compared to its movement within the ER is much slower for H2a-RFP than for CRT-GFP. This could be because of the different fates of the two proteins. Whereas H2a-RFP interacts with ERAD components such as OS-9 at the ERQC,[4,9] which would cause its retention, no such interactions are known or expected for CRT-GFP, which would be actively shuttling between the ER periphery and the ERQC.

We then looked at another quality control component, ERManI. We had shown that ERManI resides in quality control vesicles (QCVs) at the steady state, concentrating at the ERQC under ER stress.[6] We performed

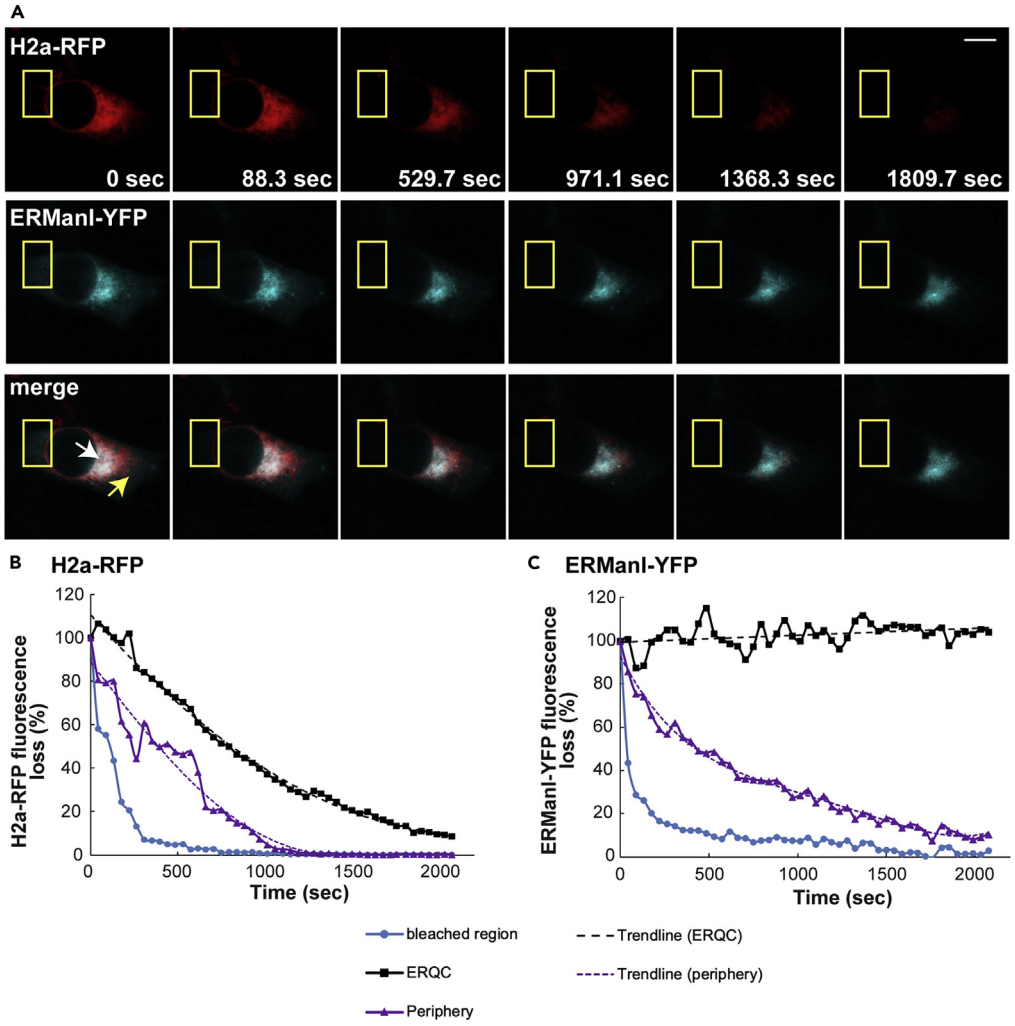

Figure 4. No recycling of ER mannosidase I from the ERQC to the ER

(A) Lac-treated NIH3T3 cells (20 μM, 3h) transfected with H2a-RFP and ERManI-YFP expressing plasmids were subjected to FLIP, repetitively bleaching in an ER periphery region (yellow rectangles) and scanned after each set of bleaching as in Figure 3C. Bar= 10 μm. Representative of 3 experiments. See Video S2.

(B and C) The percentage of the fluorescence intensity compared to the start (prior to bleaching) was calculated for each time point for H2a-RFP (B) and for ERmanI-YFP (C), indicating no measurable recycling of ERManI-YFP from the ERQC to the periphery during the time of the experiment. The trendlines in the peripheral region are polynomial (fourth order) and for H2a-RFP in the ERQC it is polynomial of the second order. See also Video S2 and Figure S4.

an FLIP experiment, similar to the one described, in NIH3T3 cells expressing H2a-RFP and ERManI-YFP under proteasomal inhibition. Although H2a-RFP trafficking resembled that of the previous experiment (Figures 4A and 4B and Video S2), the trafficking of ERManI-YFP was very different than that of H2a-RFP and CRT-GFP. The fluorescence intensity of ERManI-YFP, which appeared in a partially punctate vesicular pattern, decreased rapidly in the ER periphery during the course of the time lapse, although slower than the decrease for H2a-RFP (Figures 4C and S4). This slower decrease is likely because much of ERManI-YFP in the peripheral region is sequestered in QCVs, which can occasionally fuse with the ER. In contrast, ERManI-YFP fluorescence intensity barely changed in the ERQC, even after 30 min, double the time of the experiment in Figures 3C–3F, suggesting that it does not recycle back to the ER periphery.

Involvement of COPI and COPII coats in the trafficking to the ERQC and back

Given the results of the time lapse experiments, which indicate non-diffusive trafficking from the ERQC to the peripheral ER, consistent with vesicular trafficking, we tested the involvement of vesicular coats. We

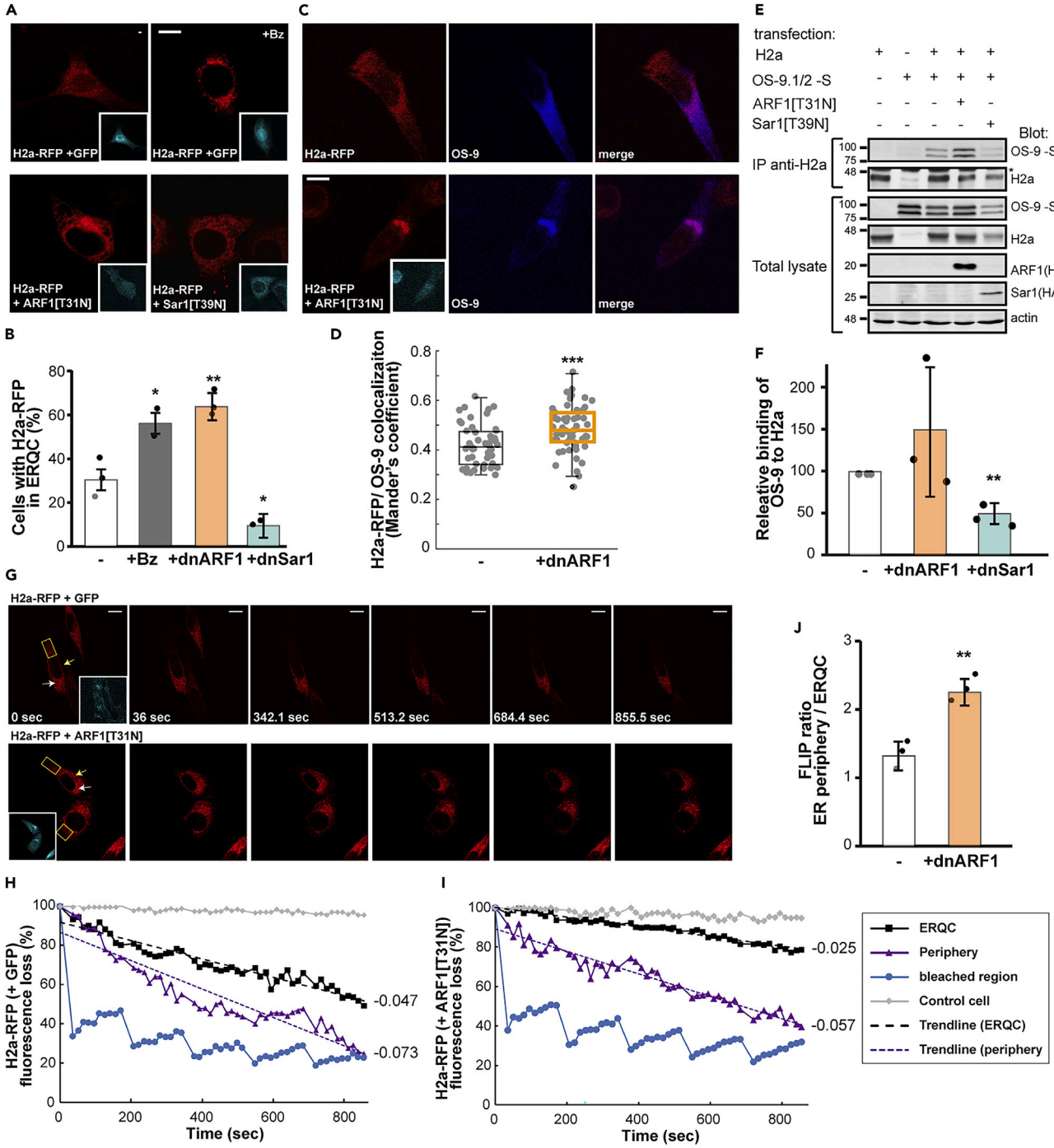

Figure 5. Vesicular coats are involved in trafficking from the peripheral ER to the ERQC and back

(A and B) NIH3T3 cells transiently expressing H2a-RFP together with GFP, ARF1[T31N]-GFP (dnARF1) or Sar1[T39N]-IRES-GFP (dnSar1). Where indicated, cells were treated for 3 h with Bz (1 μM). Bar= 10 μm. The graph shows percent of cells with ERQC accumulation of H2a-RFP, average of three independent experiments ±SD, which increased +Bz and +dnARF1, and decreased + dnSar1. p values +Bz versus control = 0.05, +dnARF1 versus control = 0.005, +dnSar1 versus control = 0.05.

(C and D) NIH3T3 cells expressing H2a-RFP and S-tagged OS-9.½, with or without ARF1[T31N]-GFP fixed and stained with anti-S-tag antibody and goat anti-mouse IgG Dy649. Bar= 10 μm. Mander's coefficients indicate that dnARF1 increased H2a-RFP colocalization with OS-9. The graph is a boxplot with inclusive medians of 3 independent experiments (~30 cells per experiment); box height = IQR; horizontal bar in the box = median; whiskers extend to the farthest value smaller than 1.5xIQR. p value = 0.0003.

(E) Immunoprecipitation with anti-H2a of lysates of HEK293 cells expressing H2a together with combinations of OS-9.1/2-S, ARF1[T31N]-HA or Sar1[T39N]-HA, as indicated. Immunoprecipitates and 10% of the total lysates were immunoblotted with anti-S-tag and anti-H2a. Total lysates were also immunoblotted

Figure 5. *Continued*

with antibodies against HA (to detect ARF1 and Sar1 constructs) and actin (loading control). The asterisk indicates a band of heavy chain. MW markers in kDa are on the left.

(F) The graph shows increased coimmunoprecipitation of OS-9 with H2a under COPI interference and decreased under COPII interference. Values are relative to control (=100), normalized by total H2a and total OS-9, average of 3 independent experiments ±SD. p value +dnSar1 versus control = 0.002.

(G–I) NIH3T3 cells transiently expressing H2a-RFP together with GFP or ARF1[T31N]-GFP were repetitively bleached in an ER periphery region (yellow rectangles) and scanned after each set of bleaching as in Figure 3C. Bars= 10μm.

(J) Ratio between the FLIP curve slopes (calculated from linear trendlines) in the ER periphery compared to the ERQC, average of 3 independent experiments ±SD. p value = 0.004. ARF1[T31N]-GFP slowed down considerably recycling from the ERQC to the periphery.

assessed the effect of overexpression of dominant-negative mutants of ARF1 (ARF1[T31N]) and Sar1 (Sar1[T39N]), which affect COPI and COPII coats respectively,[18,19] on the localization of H2a-RFP. Similarly to treatment with Bz, ARF1[T31N] caused juxtanuclear accumulation of H2a-RFP (Figures 5A and 5B), which was confirmed to be in the ERQC, by comparing with the ERQC localization of OS-9[4] (Figures 5C and 5D). In contrast, Sar1[T39N] reduced the number of cells showing spontaneous juxtanuclear accumulation of H2a-RFP (Figures 5A and 5B). A co-immunoprecipitation experiment of H2a with OS-9 showed a reduced interaction in the presence of Sar1[T39N] (Figures 5E and 5F). H2a showed a trend of increased interaction with OS-9 in the presence of ARF1[T31N], although the effect was not statistically significant.

Altogether these results suggest that COPII is necessary for trafficking of the ERAD substrate from the peripheral ER to the ERQC and interaction with OS-9, whereas COPI appears to facilitate recycling from the ERQC to the peripheral ER. To test directly the involvement of COPI in the recycling, we performed an FLIP experiment on H2a-RFP, but examining now the influence of ARF1[T31N]. Recycling from the ERQC to the periphery was strongly slowed down by ARF1[T31N] (Figures 5G–5I and Videos S3 and S4). The ratio between the fluorescence loss rates in the ER periphery and in the ERQC was almost 2-fold higher in the presence of ARF1[T31N] when averaging cells from repeat experiments (Figure 5J).

The effect on the compartmentalization by interference with COPII was also studied using iodixanol gradients. Overexpression of Sar1[T39N] caused a shift of H2a from heavier fractions (peaking around fractions 6-7) to lighter fractions (peaking around fractions 4-5) (Figures 6A and 6B). A certain amount also appeared in the heavier fraction 9, possibly indicating retention in the rough ER.[4] Overall there was a reduction in the amount of H2a in the heavier fractions (fractions 6 to 9, which include the ERQC) from 92% of the total protein in the absence of Sar1[T39N] to 41% in its presence (Figure 6C). To discard the possibility that this is an indirect effect because of the long-term (24h) interference by Sar1[T39N], a similar experiment was done but using short-term (1h) incubation with the PKA inhibitor H89, which inhibits COPII vesicular trafficking.[20] Cells were incubated with or without Bz (1 μM) for 3h with the addition of H89 (50 μM) for the last hour. The results were similar to those obtained with Sar1[T39N]. There was a reduction of H2a in ERQC fractions, from 95% in untreated cells to 47% in cells treated with H89, and in the presence of Bz from 100% to 60% with H89 (Figures 6D–6G).

We wondered whether a different type of ERAD substrate, a soluble luminal misfolded protein, human α1-antitrypsin variant null Hong Kong (NHK),[21] would show a similar effect of interference with COPII. Indeed, there was a similar reduction of NHK-HA in ERQC fractions, from 77% in untreated cells to 57% in cells treated with H89, and in the presence of Bz from 88% to 65% with H89 (Figures 6H–6K).

It is important to note that in no case was there any noticeable ERAD substrate in Golgi fractions (peaking around fractions 1-2 as indicated by the Golgi markers Cab45 or GM130, Figures 6 and S5).

COPI and COPII are involved in the regulation of misfolded protein targeting to ERAD.

The requirement of COPII function for efficient interaction of the ERAD substrate with the HRD1-SEL1L-associated OS-9 suggested that it may also regulate its targeting to ubiquitination and proteasomal degradation. To minimize indirect effects of long-term expression of the dominant negative constructs, we incubated cells for 3h with brefeldin A (BFA) (5 μg/mL), a known inhibitor of COPI vesicular transport, or H89 (100 μM). To increase the specificity and sensitivity we coexpressed myc-tagged ubiquitin. Ubiquitinated H2a was much increased, as expected, by incubation of the cells with Bz (Figure 7A). Treatment with H89 reduced this signal, consistent with less availability of the protein at the ERQC for

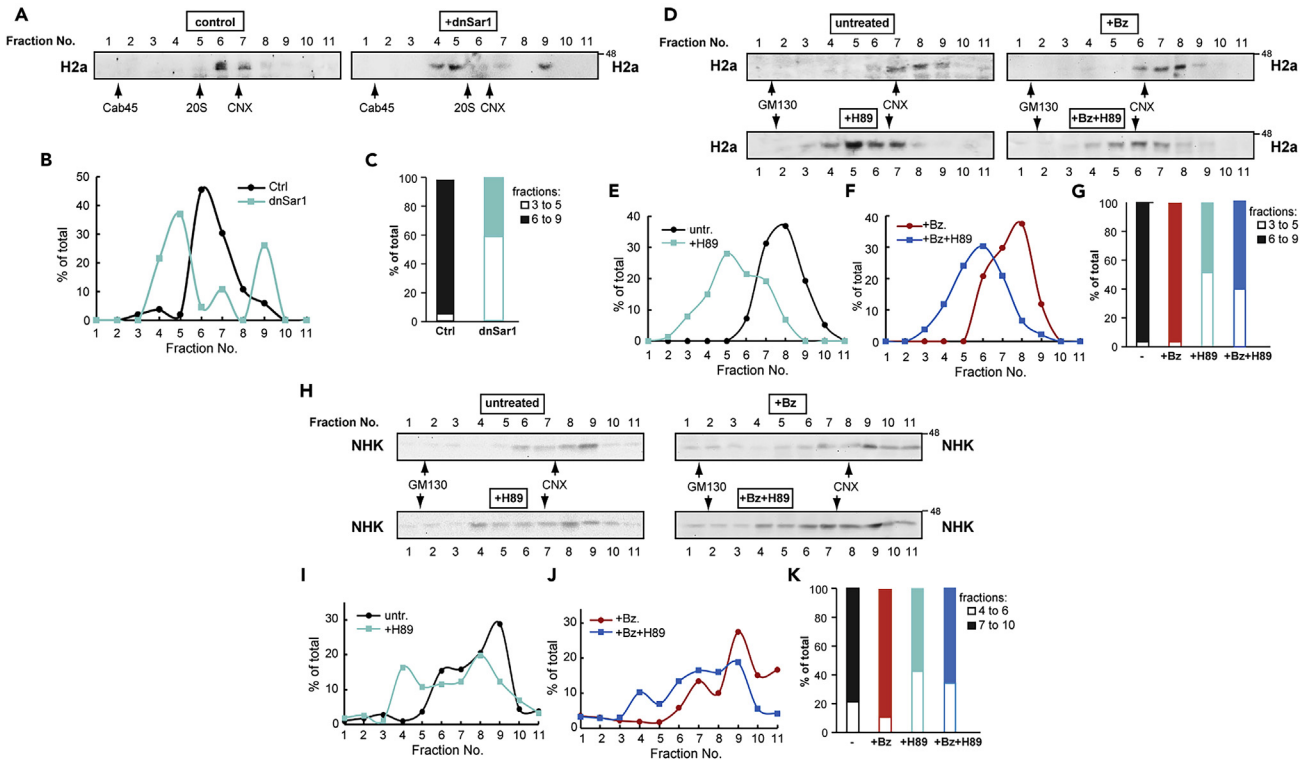

Figure 6. Interference with COPII inhibits ERAD substrate accumulation in the ERQC

(A) Homogenates from HEK293 cells expressing H2a with or without Sar1[T39N]-HA (dnSar1) were loaded on an iodixanol gradient (10%–34%) as indicated in STAR Methods. Eleven fractions were collected from the top to the bottom, run on 12% SDS-PAGE and immunoblotted with anti-H2a, anti-Cab45 (Golgi marker), anti-20S and anti-CNX antibodies (peak fractions indicated with arrows). The results shown are representative of 3 independent experiments.

(B) After quantification, the percentage of total H2a in each fraction was plotted.

(C) Comparison between the percentage of total H2a in the sum of fractions 3 to 5 and that of fractions 6 to 9 (ERQC) shows that most H2a shifts to lighter fractions under COPII interference by dnSar1.

(D) Similar to (A), but cells expressing H2a were incubated with 50 μM H89 for 1h or 1 μM Bz for 3h, or with 1 μM Bz for 3h adding 50 μM H89 in the last hour of treatment. Anti-GM130 was used here as a Golgi marker. The results shown are representative of 3 independent experiments.

(E and F) The intensity of each band was quantified and the percentage of total H2a in each fraction was plotted and compared between the control and +H89 (E), or +Bz and +Bz + H89 (F).

(G) Comparison between the percentage of total H2a in the sum of fractions 3 to 5 and that of fractions 6 to 9 (ERQC) shows that H2a shifts to lighter fractions under COPII interference by H89 treatment.

(H) Similar to (D), but with cells expressing NHK-HA. The results shown are representative of 3 independent experiments.

(I and J) The intensity of each band was quantified and the percentage of total NHK-HA in each fraction was plotted and compared between the control and +H89 (I), or +Bz and +Bz + H89 (J).

(K) Comparison between the percentage of total NHK-HA in the sum of fractions 4 to 6 and that of fractions 7 to 10 (ERQC) shows that NHK-HA shifts to lighter fractions under COPII interference by H89 treatment.

See also Figure S5.

retrotranslocation. On the other hand, BFA also reduced the signal. This might be explained by a saturation of the ubiquitination machinery by the increased retrotranslocated species, together with a fast degradation rate, only partially inhibited by Bz. We tested directly the degradation rate by pulse-chase analysis, to examine H2a degradation over time under COPI/COPII interference. HEK293 cells transiently expressing H2a were metabolically labeled with [^{35}S]cysteine. In untreated cells, H2a degraded with time, and 28% of the labeled molecules remained after 6h of chase (Figure 7B). COPII interference with H89 inhibited the degradation, with 47% of the labeled protein remaining after 6h chase. Of interest, COPI interference with BFA accelerated the degradation, with 15% remaining after 6h, a reduction to almost half of the untreated control. We also tested the effects on the degradation of NHK-HA. In this case a cycloheximide (CHX) chase was performed, quantifying the protein remaining in an immunoblot compared to β-tubulin as a housekeeping protein. In untreated cells, 54% of NHK-HA remained after 6h of chase

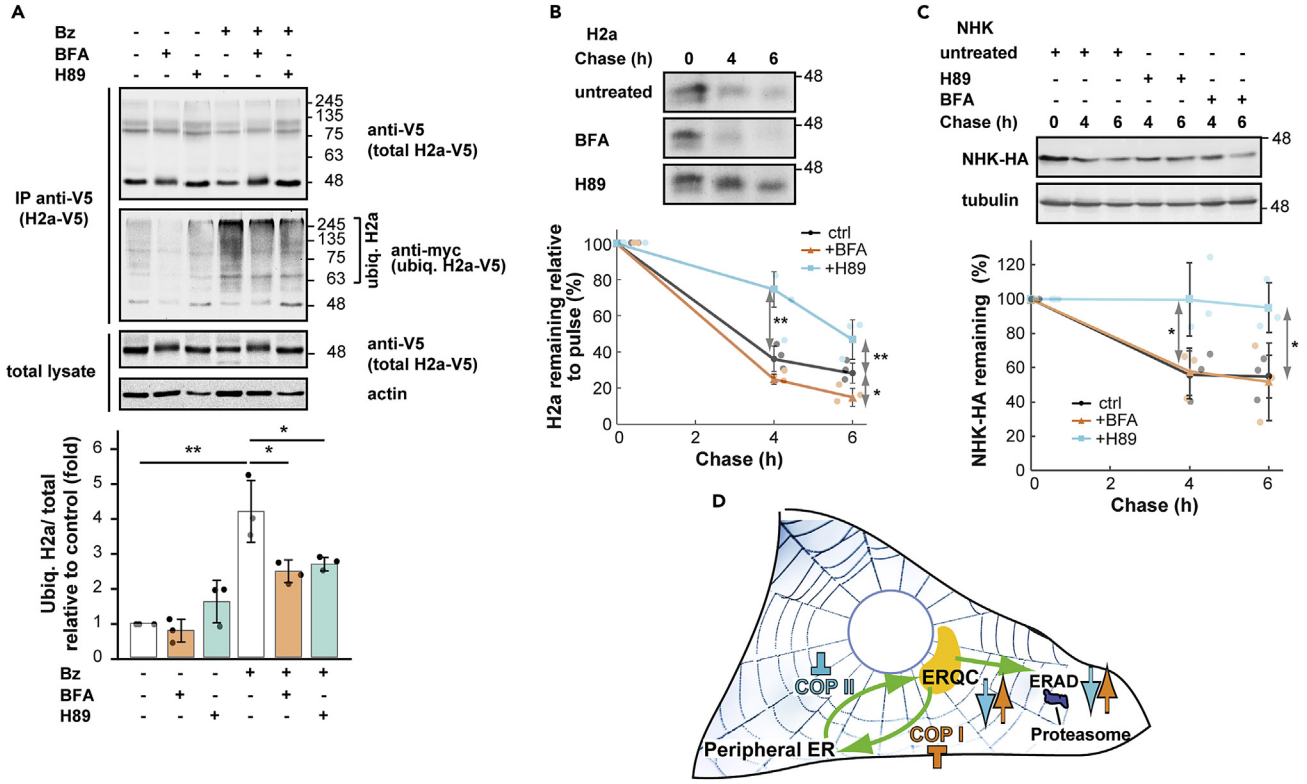

Figure 7. COPII-dependent movement from the peripheral ER to the ERQC is required for ERAD substrate ubiquitination and degradation

(A) HEK293 cells transiently expressing H2a-V5 together with myc-tagged ubiquitin were treated for 3h with or without 5 μg/ml BFA or 100 μM H89 in the presence or absence of Bz (1 μM), lysed and immunoprecipitated with rabbit anti-V5. Immunoprecipitates and 10% of total cell lysates were immunoblotted with mouse anti-V5. Immunoprecipitates were also immunoblotted with anti-myc. Values are averages of 3 independent experiments ±SD, ubiquitinated relative to total immunoprecipitated H2a, and standardized by the control (=1). p value +Bz versus control = 0.003, +BFA versus control = 0.03. +H89 versus control = 0.04.

(B) Pulse/chase of H2a. Pulse-labeling for 20 min with [^{35}S]cysteine and chase for the indicated times with or without 5 μg/ml BFA or 100 μM H89. H2a degradation (percentage remaining relative to pulse) increased under COPI interference (+BFA) and was strongly inhibited under COPII interference (+H89). The graph shows an average of 3 independent experiments ±SD. p value 6h +BFA versus control = 0.03, 6h +H89 versus control = 0.01, 4h +H89 versus control = 0.003.

(C) CHX chase of NHK-HA. HEK293 cells transiently expressing NHK-HA were treated 48h post-transfection with or without 5 μg/ml BFA or 100 μM H89 for the indicated times, lysed and immunoblotted with anti-HA or anti-β-tubulin. NHK-HA degradation (percentage remaining, normalized by β-tubulin) was strongly inhibited under COPII interference (+H89) but unaffected by COPI interference (+BFA). The graph shows an average of 3 independent experiments ±SD. p value 4h +H89 versus control = 0.04, 6h +H89 versus control = 0.02.

(D) Model of COPI and COPII involvement. COPII is involved in the movement of ERAD substrates from the peripheral ER to the ERQC. Under COPII interference this movement is inhibited. The ERAD substrates are then mostly scattered in the peripheral ER instead of accumulating in the ERQC. This leads to a slower degradation rate (light blue arrows). The recycling of ERAD substrates from the ERQC to the ER is dependent on COPI. COPI interference hinders this recycling, causing accumulation of ERAD substrates in the ERQC. Degradation of the substrates can be accelerated (orange arrows).

(Figure 7C). COPII interference with H89 strongly inhibited the degradation, with 95% of the protein remaining after 6h chase. COPI interference with BFA had no significant effect in this case, with 52% remaining after 6h.

Altogether, these results suggest involvement of COPII in the targeting of the ERAD substrate to ubiquitination and degradation. In the case of COPI, the increased degradation of H2a seen by interfering with its function suggests that it does not participate in events taking place after retrotranslocation, but rather it functions in its recycling from the ERQC to the peripheral ER, which reduces the availability of ERAD substrate molecules both for retrotranslocation and ultimately for their degradation (Figure 7D).

DISCUSSION

Previous work in our lab had characterized the ERQC as a distinct compartment, localized in the centrosomal region of the cell and not colocalizing with the Golgi apparatus, ERGIC or other organelles.[2,3] OS-9 resides constitutively in this compartment,[4,22] but ERAD substrates and other machinery components are observed to concentrate at the ERQC only on accumulation of ERAD substrates, by inhibiting their proteasomal degradation (as done here), by their overexpression or by induction of Herp, downstream of the activation of the PERK pathway.[3,4] For example, recruitment to the ERQC can be achieved by overexpressing a phosphomimetic mutant of eIF2α(S51D),[3] inhibiting eIF2α-P dephosphorylation or overexpressing Herp.[4] We had concluded from those results that even in unstressed conditions, a transient accumulation of unfolded protein molecules causes a temporary activation of the PERK pathway and an induction of Herp, leading to dynamic protein recruitment to the ERQC. Therefore, ERAD machinery components are recruited according to the demand for protein disposal and ERAD complexes might be transiently assembled only when needed, followed by disassembly and dispersal in an "ERAD cycle". We have now observed that also inhibition of COPI vesicular trafficking with a dominant-negative mutant of ARF1 causes an accumulation of the ERAD substrate H2a in the ERQC (Figure 5), suggesting that the recycling or dispersal is inhibited. Many quality control and ERAD components are recruited to the ERQC, also from the cytosolic side, including proteasomes, but some are excluded, such as the abundant chaperone BiP (Figure 1).[5]

Both glycoproteins and non-glycosylated ERAD substrates concentrate at the ERQC, as they share much of a common quality control machinery.[1,7] However, we have observed that the trafficking of CRT to the ERQC is dependent on the presence of an active lectin domain (Figure 2), and abrogated in a mutant without lectin activity,[17] suggesting that it follows the accumulation of its glycoprotein clients. CRT appears to cycle actively between the peripheral ER and the ERQC (Figure 3). In contrast, another glycoprotein quality control component, ERManI, does not recycle (Figure 4) and seems to be effectively sequestered in QCVs or in the ERQC.

We have described the QCVs as a new type of vesicles, where the mannosidases ERManI and mannosidase IA (ManIA) are normally kept segregated from their substrate glycoproteins.[6,23] Only occasionally do the glycoproteins interact with the mannosidases at the QCVs or at their fusion sites with the ER. The QCVs are dependent on COPII, but coat components were not observed on the vesicles. Future studies should determine whether the QCVs are the same carriers for the trafficking of the ERAD substrates.

Interference with COPII inhibits ERQC localization of both a membrane-bound ERAD substrate, H2a and a soluble luminal one, NHK, and inhibits their degradation (Figures 5, 6, and 7). One possibility is that the interference with COPII affects the QCVs, thus causing an inhibition of substrate interaction with the mannosidases, which reduces mannose trimming and delivery to ERAD. However, the slow dynamics of H2a-RFP to the ERQC (Figure 2) and its slow recycling (Figures 3 and 4) suggest vesicular transport of the substrate and not an indirect effect of the mannose trimming. Trafficking of ERAD substrates and recruitment of machinery components at the ERQC is also microtubule dependent.[2]

The requirement of functional vesicular trafficking for ERAD was previously reported in *Saccharomyces cerevisiae*, but the mechanism of this involvement was unclear.[24,25] The COPII-dependent sorting to an ER subdomain, named ER-associated compartment (ERAC), was found to be required for proteasomal degradation of an ERAD substrate, mutant CFTR, in *S. cerevisiae*. Perhaps the ERAC is a functional homolog of the ERQC in yeast, although there are some differences, such as the accumulation of the BiP homolog, Kar2 in the ERAC whereas BiP does not accumulate in the ERQC.[26,27]

COPI and II vesicular trafficking is traditionally associated with movement between the ER and the Golgi. However, COPII coats have recently been implicated in other pathways as well. For example, in the formation of ER whorls, which appear in certain conditions and were found to be PERK and COPII dependent.[13] COPII was also found to be involved in the initiation of the autophagic process in yeast[14,15] and mammalian cells.[28] Some interesting recent reports depart from the classical model, suggesting that COPII concentrates at the ER exit sites, creating a boundary, but does not coat the vesicular carriers.[29,30] COPII and also COPI involvement might be in the vesicle budding stage, with alternative factors possibly targeting the vesicles to different locations.[31,32]

There are reports of misfolded proteins in yeast[24,33] and mammalian cells[34,35] that are sent back to the ER from the Golgi or from the ERGIC.[36] However, in the case of H2a that we have analyzed here, it is retained in the ER and does not traffic to the Golgi nor to the ERGIC.[4,5,7,37]

Our results show that by interfering with misfolded protein delivery to the ERQC (Figures 5 and 6), interference with COPII surprisingly inhibits ERAD (Figure 7). COPII mutations are reported to cause ER stress, which has been interpreted as resulting from the accumulation of secretory proteins that cannot travel to the Golgi,[38] but an additional cause might be an outcome of ERAD inhibition.

Limitations of the study

A limitation of the study is that it focuses on one established ERAD substrate, confirming the main findings with another one, which does not determine whether the findings are universal for all substrates.

STAR★METHODS

Detailed methods are provided in the online version of this paper and include the following:

- KEY RESOURCES TABLE
- RESOURCE AVAILABILITY
  - Lead contact
  - Materials availability
  - Data and code availability
- EXPERIMENTAL MODEL AND SUBJECT DETAILS
  - Cell culture
- METHOD DETAILS
  - Materials
  - Antibodies
  - Plasmids and constructs
  - Cell culture, media and transfections
  - Microsome isolation and gradient fractionation
  - Metabolic labeling
  - Immunoprecipitation and immunoblotting
  - Immunofluorescence microscopy
  - Live cell imaging
- QUANTIFICATION AND STATISTICAL ANALYSIS

SUPPLEMENTAL INFORMATION

Supplemental information can be found online at https://doi.org/10.1016/j.isci.2023.106232.

ACKNOWLEDGMENTS

We would like to thank Erik Snapp, Ariel Stanhill, Michal Sharon, Ron Kopito and Maurizio Molinari for plasmids and reagents. Work was supported by grants (1593/16 and 2577/20) from the Israel Science Foundation (GZL).

AUTHOR CONTRIBUTIONS

Conceptualization: G.Z.L. Investigation: N.O-S., C.C., H.S., N.M., C.P., M.S. Supervision: G.Z.L. Writing: N.O-S. and G.Z.L. Review and editing: G.Z.L., N.O-S., C.C., H.S., C.P., and M.S.

DECLARATION OF INTERESTS

The authors declare no competing interests.

Received: September 28, 2022
Revised: January 9, 2023
Accepted: February 14, 2023
Published: February 19, 2023

REFERENCES

1. Benyair, R., Ogen-Shtern, N., and Lederkremer, G.Z. (2015). Glycan regulation of ER-associated degradation through compartmentalization. Semin. Cell Dev. Biol. *41*, 99–109. https://doi.org/10.1016/j.semcdb.2014.11.006.

2. Kamhi-Nesher, S., Shenkman, M., Tolchinsky, S., Fromm, S.V., Ehrlich, R., and Lederkremer, G.Z. (2001). A novel quality control compartment derived from the endoplasmic reticulum. Mol. Biol. Cell *12*, 1711–1723. https://doi.org/10.1091/mbc.12.6.1711.

3. Kondratyev, M., Avezov, E., Shenkman, M., Groisman, B., and Lederkremer, G.Z. (2007). PERK-dependent compartmentalization of ERAD and unfolded protein response machineries during ER stress. Exp. Cell Res. *313*, 3395–3407. https://doi.org/10.1016/j.yexcr.2007.07.006.

4. Leitman, J., Shenkman, M., Gofman, Y., Shtern, N.O., Ben-Tal, N., Hendershot, L.M., and Lederkremer, G.Z. (2014). Herp coordinates compartmentalization and recruitment of HRD1 and misfolded proteins for ERAD. Mol. Biol. Cell *25*, 1050–1060. https://doi.org/10.1091/mbc.E13-06-0350.

5. Shenkman, M., and Lederkremer, G.Z. (2019). Compartmentalization and selective tagging for disposal of misfolded glycoproteins. Trends Biochem. Sci. *44*, 827–836. https://doi.org/10.1016/j.tibs.2019.04.012.

6. Benyair, R., Ogen-Shtern, N., Mazkereth, N., Shai, B., Ehrlich, M., and Lederkremer, G.Z. (2015). Mammalian ER mannosidase I resides in quality control vesicles, where it encounters its glycoprotein substrates. Mol. Biol. Cell *26*, 172–184. https://doi.org/10.1091/mbc.E14-06-1152.

7. Shenkman, M., Groisman, B., Ron, E., Avezov, E., Hendershot, L.M., and Lederkremer, G.Z. (2013). A shared endoplasmic reticulum-associated degradation pathway involving the EDEM1 protein for glycosylated and nonglycosylated proteins. J. Biol. Chem. *288*, 2167–2178. https://doi.org/10.1074/jbc.M112.438275.

8. Frenkel, Z., Shenkman, M., Kondratyev, M., and Lederkremer, G.Z. (2004). Separate roles and different routing of calnexin and ERp57 in endoplasmic reticulum quality control revealed by interactions with asialoglycoprotein receptor chains. Mol. Biol. Cell *15*, 2133–2142. https://doi.org/10.1091/mbc.e03-12-0899.

9. Groisman, B., Shenkman, M., Ron, E., and Lederkremer, G.Z. (2011). Mannose trimming is required for delivery of a glycoprotein from EDEM1 to XTP3-B and to late endoplasmic reticulum-associated degradation steps. J. Biol. Chem. *286*, 1292–1300. https://doi.org/10.1074/jbc.M110.154849.

10. Barlowe, C., Orci, L., Yeung, T., Hosobuchi, M., Hamamoto, S., Salama, N., Rexach, M.F., Ravazzola, M., Amherdt, M., and Schekman, R. (1994). COPII: a membrane coat formed by Sec proteins that drive vesicle budding from the endoplasmic reticulum. Cell *77*, 895–907. https://doi.org/10.1016/0092-8674(94)90138-4.

11. Letourneur, F., Gaynor, E.C., Hennecke, S., Démollière, C., Duden, R., Emr, S.D., Riezman, H., and Cosson, P. (1994). Coatomer is essential for retrieval of dilysine-tagged proteins to the endoplasmic reticulum. Cell *79*, 1199–1207. https://doi.org/10.1016/0092-8674(94)90011-6.

12. Orci, L., Palmer, D.J., Ravazzola, M., Perrelet, A., Amherdt, M., and Rothman, J.E. (1993). Budding from Golgi membranes requires the coatomer complex of non-clathrin coat proteins. Nature *362*, 648–652. https://doi.org/10.1038/362648a0.

13. Xu, F., Du, W., Zou, Q., Wang, Y., Zhang, X., Xing, X., Li, Y., Zhang, D., Wang, H., Zhang, W., et al. (2021). COPII mitigates ER stress by promoting formation of ER whorls. Cell Res. *31*, 141–156. https://doi.org/10.1038/s41422-020-00416-2.

14. Cui, Y., Parashar, S., and Ferro-Novick, S. (2020). A new role for a COPII cargo adaptor in autophagy. Autophagy *16*, 376–378. https://doi.org/10.1080/15548627.2019.1699347.

15. Cui, Y., Parashar, S., Zahoor, M., Needham, P.G., Mari, M., Zhu, M., Chen, S., Ho, H.C., Reggiori, F., Farhan, H., et al. (2019). A COPII subunit acts with an autophagy receptor to target endoplasmic reticulum for degradation. Science *365*, 53–60. https://doi.org/10.1126/science.aau9263.

16. Leitman, J., Ulrich Hartl, F., and Lederkremer, G.Z. (2013). Soluble forms of polyQ-expanded huntingtin rather than large aggregates cause endoplasmic reticulum stress. Nat. Commun. *4*, 2753. https://doi.org/10.1038/ncomms3753.

17. Snapp, E.L., Sharma, A., Lippincott-Schwartz, J., and Hegde, R.S. (2006). Monitoring chaperone engagement of substrates in the endoplasmic reticulum of live cells. Proc. Natl. Acad. Sci. USA *103*, 6536–6541. https://doi.org/10.1073/pnas.0510657103.

18. Dascher, C., and Balch, W.E. (1994). Dominant inhibitory mutants of ARF1 block endoplasmic reticulum to Golgi transport and trigger disassembly of the Golgi apparatus. J. Biol. Chem. *269*, 1437–1448.

19. Weissman, J.T., Plutner, H., and Balch, W.E. (2001). The mammalian guanine nucleotide exchange factor mSec12 is essential for activation of the Sar1 GTPase directing endoplasmic reticulum export. Traffic *2*, 465–475. https://doi.org/10.1034/j.1600-0854.2001.20704.x.

20. Aridor, M., and Balch, W.E. (2000). Kinase signaling initiates coat complex II (COPII) recruitment and export from the mammalian endoplasmic reticulum. J. Biol. Chem. *275*, 35673–35676. https://doi.org/10.1074/jbc.C000449200.

21. Ferris, S.P., Jaber, N.S., Molinari, M., Arvan, P., and Kaufman, R.J. (2013). UDP-glucose:glycoprotein glucosyltransferase (UGGT1) promotes substrate solubility in the endoplasmic reticulum. Mol. Biol. Cell *24*, 2597–2608. https://doi.org/10.1091/mbc.E13-02-0101.

22. Ron, E., Shenkman, M., Groisman, B., Izenshtein, Y., Leitman, J., and Lederkremer, G.Z. (2011). Bypass of glycan-dependent glycoprotein delivery to ERAD by up-regulated EDEM1. Mol. Biol. Cell *22*, 3945–3954. https://doi.org/10.1091/mbc.E10-12-0944.

23. Ogen-Shtern, N., Avezov, E., Shenkman, M., Benyair, R., and Lederkremer, G.Z. (2016). Mannosidase IA is in quality control vesicles and participates in glycoprotein targeting to ERAD. J. Mol. Biol. *428*, 3194–3205. https://doi.org/10.1016/j.jmb.2016.04.020.

24. Caldwell, S.R., Hill, K.J., and Cooper, A.A. (2001). Degradation of endoplasmic reticulum (ER) quality control substrates requires transport between the ER and Golgi. J. Biol. Chem. *276*, 23296–23303. https://doi.org/10.1074/jbc.M102962200.

25. Taxis, C., Vogel, F., and Wolf, D.H. (2002). ER-golgi traffic is a prerequisite for efficient ER degradation. Mol. Biol. Cell *13*, 1806–1818. https://doi.org/10.1091/mbc.01-08-0399.

26. Fu, L., and Sztul, E. (2003). Traffic-independent function of the Sar1p/COPII machinery in proteasomal sorting of the cystic fibrosis transmembrane conductance regulator. J. Cell Biol. *160*, 157–163. https://doi.org/10.1083/jcb.200210086.

27. Kakoi, S., Yorimitsu, T., and Sato, K. (2013). COPII machinery cooperates with ER-localized Hsp40 to sequester misfolded membrane proteins into ER-associated compartments. Mol. Biol. Cell *24*, 633–642. https://doi.org/10.1091/mbc.E12-08-0639.

28. Ge, L., Wilz, L., and Schekman, R. (2015). Biogenesis of autophagosomal precursors for LC3 lipidation from the ER-Golgi intermediate compartment. Autophagy *11*, 2372–2374. https://doi.org/10.1080/15548627.2015.1105422.

29. Shomron, O., Nevo-Yassaf, I., Aviad, T., Yaffe, Y., Zahavi, E.E., Dukhovny, A., Perlson, E., Brodsky, I., Yeheskel, A., Pasmanik-Chor, M., et al. (2021). COPII collar defines the boundary between ER and ER exit site and does not coat cargo containers. J. Cell Biol. *220*, e201907224. https://doi.org/10.1083/jcb.201907224.

30. Weigel, A.V., Chang, C.-L., Shtengel, G., Xu, C.S., Hoffman, D.P., Freeman, M., Iyer, N., Aaron, J., Khuon, S., Bogovic, J., et al. (2021). ER-to-Golgi protein delivery through an interwoven, tubular network extending from ER. Cell *184*, 2412–2429.e16. https://doi.org/10.1016/j.cell.2021.03.035.

31. Phuyal, S., and Farhan, H. (2021). Want to leave the ER? We offer vesicles, tubules, and tunnels. J. Cell Biol. *220*, e202104062. https://doi.org/10.1083/jcb.202104062.

32. Westrate, L.M., Hoyer, M.J., Nash, M.J., and Voeltz, G.K. (2020). Vesicular and uncoated

Rab1-dependent cargo carriers facilitate ER to Golgi transport. J. Cell Sci. *133*, jcs239814. https://doi.org/10.1242/jcs.239814.

33. Vashist, S., Kim, W., Belden, W.J., Spear, E.D., Barlowe, C., and Ng, D.T. (2001). Distinct retrieval and retention mechanisms are required for the quality control of endoplasmic reticulum protein folding. J. Cell Biol. *155*, 355–368. https://doi.org/10.1083/jcb.200106123.

34. Hellerschmied, D., Serebrenik, Y.V., Shao, L., Burslem, G.M., and Crews, C.M. (2019). Protein folding state-dependent sorting at the Golgi apparatus. Mol. Biol. Cell *30*, 2296–2308. https://doi.org/10.1091/mbc.E19-01-0069.

35. Hsu, V.W., Yuan, L.C., Nuchtern, J.G., Lippincott-Schwartz, J., Hammerling, G.J., and Klausner, R.D. (1991). A recycling pathway between the endoplasmic reticulum and the Golgi apparatus for retention of unassembled MHC class I molecules. Nature *352*, 441–444. https://doi.org/10.1038/352441a0.

36. Sirkis, D.W., Aparicio, R.E., and Schekman, R. (2017). Neurodegeneration-associated mutant TREM2 proteins abortively cycle between the ER and ER-Golgi intermediate compartment. Mol. Biol. Cell *28*, 2723–2733. https://doi.org/10.1091/mbc.E17-06-0423.

37. Shenkman, M., Ayalon, M., and Lederkremer, G.Z. (1997). Endoplasmic reticulum quality control of asialoglycoprotein receptor H2a involves a determinant for retention and not retrieval. Proc. Natl. Acad. Sci. USA *94*, 11363–11368. https://doi.org/10.1073/pnas.94.21.11363.

38. Lu, C.L., and Kim, J. (2020). Consequences of mutations in the genes of the ER export machinery COPII in vertebrates. Cell Stress Chaperones *25*, 199–209. https://doi.org/10.1007/s12192-019-01062-3.

39. Tolchinsky, S., Yuk, M.H., Ayalon, M., Lodish, H.F., and Lederkremer, G.Z. (1996). Membrane-bound versus secreted forms of human asialoglycoprotein receptor subunits - role of a juxtamembrane pentapeptide. J. Biol. Chem. *271*, 14496–14503. https://doi.org/10.1074/jbc.271.24.14496.

40. Scherer, P.E., Lederkremer, G.Z., Williams, S., Fogliano, M., Baldini, G., and Lodish, H.F. (1996). Cab45, a novel (Ca2+)-binding protein localized to the Golgi lumen. J. Cell Biol. *133*, 257–268. https://doi.org/10.1083/jcb.133.2.257.

41. Sukenik, S., Braunstein, I., and Stanhill, A. (2021). An arsenite relay between PSMD14 and AIRAP enables revival of proteasomal DUB activity. Biomolecules *11*, 1317. https://doi.org/10.3390/biom11091317.

42. Sharma, N., Patel, C., Shenkman, M., Kessel, A., Ben-Tal, N., and Lederkremer, G.Z. (2021). The Sigma-1 receptor is an ER-localized type II membrane protein. J. Biol. Chem. *297*, 101299. https://doi.org/10.1016/j.jbc.2021.101299.

43. Hendershot, L.M., Wei, J.Y., Gaut, J.R., Lawson, B., Freiden, P.J., and Murti, K.G. (1995). In vivo expression of mammalian BiP ATPase mutants causes disruption of the endoplasmic reticulum. Mol. Biol. Cell *6*, 283–296. https://doi.org/10.1091/mbc.6.3.283.

44. Furman, C., Short, S.M., Subramanian, R.R., Zetter, B.R., and Roberts, T.M. (2002). DEF-1/ASAP1 is a GTPase-activating protein (GAP) for ARF1 that enhances cell motility through a GAP-dependent mechanism. J. Biol. Chem. *277*, 7962–7969. https://doi.org/10.1074/jbc.M109149200.

45. Moorhead, A.M., Jung, J.Y., Smirnov, A., Kaufer, S., and Scidmore, M.A. (2010). Multiple host proteins that function in phosphatidylinositol-4-phosphate metabolism are recruited to the chlamydial inclusion. Infect. Immun. *78*, 1990–2007. https://doi.org/10.1128/iai.01340-09.

46. Avezov, E., Frenkel, Z., Ehrlich, M., Herscovics, A., and Lederkremer, G.Z. (2008). Endoplasmic reticulum (ER) mannosidase I is compartmentalized and required for N-glycan trimming to Man5-6GlcNAc2 in glycoprotein ER-associated degradation. Mol. Biol. Cell *19*, 216–225. https://doi.org/10.1091/mbc.e07-05-0505.

STAR★METHODS

KEY RESOURCES TABLE

REAGENT or RESOURCE	SOURCE	IDENTIFIER
Antibodies		
Rabbit anti H2a	Tolchinski et al.[39]	N/A
Rabbit anti-Cab45	Scherer et al.[40]	N/A
Rabbit anti-BiP	Sigma-Aldrich	Cat#G8918 RRID:AB_477030, G9043 RRID:AB_2279879
Rabbit anti-GM130	Abcam	Cat#AB52649 RRID:AB_880266
Rabbit anti-CNX	Sigma-Aldrich	Cat#C4731 RRID:AB_476845
Rabbit anti-dsRED	MBL	Cat#PM005 RRID:AB_591279
Rabbit anti-19S	Thermo scientific	Cat#PA1-964 RRID:AB_325947
Rabbit anti-20S	Abcam	Cat#ab22673 RRID:AB_2268907
Mouse anti-HA	BioLegend	Cat#901514 RRID:AB_2565336
Mouse anti-HA	Sigma-Aldrich	Cat#H3663 RRID:AB_262051
Mouse anti-actin	Sigma-Aldrich	Cat#A3853 RRID:AB_2765344
Mouse anti-tubulin	Sigma-Aldrich	Cat#T4026 RRID:AB_477577
Mouse anti-S-tag	Novagen	Cat#71549-3 RRID:AB_11210600
Mouse anti-V5	GenScript	Cat#A01724 RRID:AB_2622216
Rabbit anti-V5	Cell Signaling	Cat#13202, RRID:AB_2687461
Mouse anti-Myc	Cell Signaling	Cat# 2276, RRID:AB_331783
Rabbit anti-GFP	Santa Cruz Biotechnology	Cat#sc-8334 RRID:AB_641123
Goat anti-mouse IgG-HRP	Jackson ImmunoResearch Labs	Cat#115-035-166 RRID:AB_2338511
Goat anti-rabbit IgG-HRP	Jackson ImmunoResearch Labs	Cat#111-035-144 RRID:AB_2307391
Goat anti-mouse IgG Dy649	Jackson ImmunoResearch Labs	discontinued
Chemicals, peptides, and recombinant proteins		
Cycloxeximide	Sigma	Cat#1810
ALLN	Sigma	Cat#A6185
MG132	Calbiochem	Cat# 133407-82-6
Bortezomib	Sigma	Cat#179324-69-7
H89	Sigma	Cat#B-1427
Lactacystin	Calbiochem	Cat#L-6785
Protein A-Sepharose	Repligen	Cat#IPA300S
DAPI (4′,6- diamidino-2- phenylindole)	Sigma	Cat#F6057
DL-Dithiothreitol	Sigma	Cat#D9779
OptiPrep™ Density Gradient Medium	Sigma	Cat#D1556
[^{35}S]Cys	PerkinElmer	Cat#NEG772007MC
Brefeldin A	Sigma	Cat#B6542
cOmplete™ Protease Inhibitor Cocktail	Roche	Cat#11697498001
ViaFect™ Transfection Reagent	Promega	Cat#E4981
DMEM	Gibco	Cat# 41965-039
Trypsin	Biological Ind., Israel	Cat# 04-007- 1A

(*Continued on next page*)

Continued

REAGENT or RESOURCE	SOURCE	IDENTIFIER
Experimental models: Cell lines		
NIH 3T3	ATCC	Cat#CRL-1658
CHO	ATCC	Cat#CCL-61
HEK 293	ATCC	Cat#CRL-1573
Recombinant DNA		
pCDNA3.1 - psmd14-YFP	A. Stanhill, (Open Univ., Israel)[41]	N/A
pEGFP-C1 - CRT-GFP	E. Snapp, (Janelia)	N/A
pEGFP-C1 - CRT(Y108F)-GFP	E. Snapp, (Janelia)	N/A
pcDNA1 - H2a	Kamhi-Nesher et al.[2]	N/A
pcDNA3.1(+) - BiP-GFP	Benyair et al.[6]	N/A
pcDNA3.1(+) - H2a-RFP	Benyair et al.[6]	N/A
pcDNA3.1(+) - S-tagged-OS-9.1	Benyair et al.[6]	N/A
pcDNA3.1(+) - S-tagged-OS-9.2	Benyair et al.[6]	N/A
ERManI-YFP	This paper	N/A
pTARGET - Sar1[T39N]-HA	Benyair et al.[6]	N/A
IRES-GFP - Sar1[T39N]-HA	Benyair et al.[6]	N/A
pcDNA3.1(+) - ARF1[T31N]-HA	Addgene	#10833
EGFP N3 - ARF1[T31N]-GFP	Addgene	#49580
pBABE-puro	Addgene	#1764
H2a-BAP-V5	Sharma et al.[42]	N/A
pUB221 - Myc-UB8	R. Kopito (Stanford University)	N/A
pcDNA3.1(+) - NHK-HA	M. Molinari (IRB, Switzerland)	N/A

RESOURCE AVAILABILITY

Lead contact

Gerardo Z. Lederkremer. gerardol@tauex.tau.ac.il.

Materials availability

All the unique reagents developed in this work are available upon request.

Data and code availability

- All data reported in this paper will be shared by the lead contact upon request.
- This paper does not report original code.
- Any additional information required to reanalyze the data reported in this paper is available from the lead contact upon request.

EXPERIMENTAL MODEL AND SUBJECT DETAILS

Cell culture

NIH 3T3, CHO and HEK 293 cells were from ATCC.

METHOD DETAILS

Materials

ALLN, MG132, Bz, H89 and biotin were from Sigma. Lac was from Calbiochem. Protein A-Sepharose was from Repligen (Needham, MA). Other common reagents were from Sigma-Aldrich.

Antibodies

Rabbit polyclonal anti-H2a amino-terminal and carboxy-terminal antibodies were the one used in previous studies.[39] Rabbit polyclonal anti-Cab45 carboxy-terminal antibody was described in.[40] Rabbit polyclonal anti-BiP carboxy-terminal antibody[43] from Linda Hendershot (St. Jude Hospital) was used before.[4] Rabbit polyclonal anti-GM130 was from BioLegend, anti-CNX from Sigma and anti-dsRED from MBL. Rabbit polyclonal anti-19S proteasome from Thermo scientific and anti-20S proteasome from Abcam and were kind gifts from Michal Sharon, Weizmann Institute.

Mouse monoclonal anti-HA was from Sigma or from BioLegend, anti-actin and anti-β-tubulin from Sigma, anti-S-tag from Novagen, anti-V5 from GenScript and anti-GFP from Santa Cruz Biotechnology. Goat anti-mouse IgG-HRP, goat anti-rabbit IgG-HRP and goat anti-mouse IgG Dy649 were from Jackson-ImmunoResearch Labs.

Plasmids and constructs

psmd14-YFP was a kind gift of A. Stanhill, (Open Univ., Israel)).[41] CRT-GFP and mutCRT-GFP: CRT and CRT(Y108F) expressed in pEGFP-C1 were kind gifts from Erik Snapp, (Janelia).[17] H2a in pcDNA1 was described before.[2] Human α1-antitrypsin NHK-HA in pcDNA3.1 was a kind gift of Maurizio Molinari (IRB, Bellinzona, Switzerland).[21] BiP-GFP, H2a-RFP, S-tagged-OS-9.1 and S-tagged-OS-9.2 in pcDNA3.1(+) were used before.[3,4,6,23] ERManI-YFP was constructed with human ERManI cloned into peYFP-N1 (Clontech) using Hind III and Xma I yielding ERManI fused on its C-terminus to YFP through a 6 amino acid flexible linker (SGGGGS). Sar1[T39N]-HA in pTARGET or in IRES-GFP (Clontech) were used before.[6] ARF1 [T31N]-HA in pcDNA3.1(+),[44] ARF1[T31N]-GFP[45] and pBABE-puro were from Addgene. H2a-BAP-V5 was used before.[42]

Cell culture, media and transfections

NIH 3T3, CHO and HEK293 cells were grown in DMEM supplemented with 10% bovine calf serum at 37 °C under 5% CO_2. Transfections of NIH 3T3 and CHO cells were carried out using a Neon MP-100 microporator system (Life Technologies, Carlsbad, CA). Transfection of HEK293 cells was performed using the calcium phosphate method. Stable CHO cell lines expressing CRT-GFP or CRT(Y108F)-GFP were obtained by co-transfection with pBABE-puro (Addgene) and selection with puromycin.

Microsome isolation and gradient fractionation

Cells were homogenized by passing through a 25-gauge needle 5 times followed by 30 strokes with a Dounce homogenizer (Kontes glass co.) in an iso-osmotic buffer consisting of 10 mM Hepes (pH 7.4) and 250 mM sucrose. Debris and nuclei were pelleted by centrifugation at 1,000xg at 4°C for 10 minutes. Then the supernatants were loaded on top of a iodixanol gradient (10 to 34%) as previously described.[23] The gradients were ultra-centrifuged at 24,000 rpm (~98,500g, Beckman SW41 rotor) at 4°C for 16 hours. Eleven fractions were collected from top to bottom and subjected to gel electrophoresis followed by immunoblotting.

Metabolic labeling

Subconfluent (90%) cell monolayers in 60-mm dishes were labeled for 30 min with [^{35}S]Cys and chased for different periods of time with normal DMEM plus 10% FCS, lysed, and immunoprecipitated with anti-H2a carboxy-terminal antibody as described previously.[23,39] Quantitation was performed in a Fujifilm FLA 5100 phosphorimager (Tokyo, Japan).

Immunoprecipitation and immunoblotting

Cell lysis and immunoprecipitation were done as described before.[39] Briefly, subconfluent (90%) cell monolayers cells were lysed with 1% Triton X-100 and 0.5% sodium deoxycholate in PBS in the presence of cOmplete™ Protease Inhibitor Cocktail for 30 min on ice. After pelleting of nuclei, lysates were immunoprecipitated with protein A-Sepharose and the appropriate antibody, incubated at 4 °C with rotation for 16 h, followed by three washes with 0.5% Triton X-100, 0.25% sodium deoxycholate and 0.5% SDS in PBS and once with PBS. Samples were boiled in sample buffer for 5 minutes and run on SDS-PAGE under reducing conditions. Transfer to a nitrocellulose membrane, immunoblotting, detection by ECL, and quantitation in a Bio-Rad ChemiDocXRS Imaging System (Hercules, CA) were done as described previously.[22] Quantity one or ImageJ software were used for the quantitation.

Immunofluorescence microscopy

Immunofluorescence was performed as described previously.[2,16,46] Briefly, cells grown for 24 h after transfection on coverslips in 24-well plates were fixed with 3% paraformaldehyde for 30 min, incubated with 50mM glycine in PBS, and permeabilized with 0.5% Triton X-100. After blocking with normal goat IgG in PBS/2% BSA, they were exposed to primary antibody for 60 min, washed and incubated for 30 min with a secondary antibody, followed by washes and staining of nuclei with DAPI. Specimens were observed with a Leica DMRBE microscope, or confocal microscopy on a Zeiss laser scanning confocal microscope (LSM 510; Carl Zeiss, Jena, Germany). ImageJ was used to quantify fluorescence intensity and to calculate Pearson's and Mander's coefficients (using JACOP) for colocalization studies. To quantify ERQC fluorescence as percent of total in the cell (% fluorescence in ERQC) the ERQC was identified by an accumulation of H2a-RFP. For each channel, fluorescence intensity and area were measured in the ERQC region and in the whole cell and the ratio of intensity*area between the ERQC and the whole cell was calculated using ImageJ. To quantify the percent of cells with ERQC accumulation, cells showing visually ERQC accumulation were counted and their ratio to the total fluorescent cell number in the sample was calculated.

Live cell imaging

Cells were transfected and grown in 35mm culture dishes on 25mm coverslips. 24 hours post-transfection images were captured using a Zeiss LSM 510 Meta confocal microscope. Cells were kept in a stage incubator which provides tissue culture conditions (37°C, CO_2). For FLIP experiments, GFP bleaching was achieved with an argon laser at a wavelength of 488nm, 100% output. RFP bleaching was achieved with solid state laser at a wavelength of 561nm, 15% output. Bleaching was done repetitively in an ER periphery region and scanned after each set of bleaching (200 iterations at each time point). The experiment with cells expressing H2a-RFP together with GFP or ARF1[T31N]-GFP was done in a Leica SP8 microscope with RFP bleaching at 561nm and 10% output, done repetitively with 20 iterations at each time point. Analyses were performed in ImageJ software.

QUANTIFICATION AND STATISTICAL ANALYSIS

The results are expressed as average $\pm$ SD or mean $\pm$ SEM as indicated. Student's t-test (two-tailed) was used to compare the averages of two groups. Statistical significance was determined at $P<0.05$ (*), $P<0.01$ (**), $P<0.001$ (***).